Research Paper

Nanoscale "fluorescent stone": Luminescent Calcium Fluoride Nanoparticles as Theranostic Platforms

Zhanjun Li*, Yuanwei Zhang*, Ling Huang, Yuchen Yang, Yang Zhao, Ghida El-Banna, Gang Han✉

Department of Biochemistry and Molecular Pharmacology, University of Massachusetts Medical School, Worcester, Massachusetts 01605 (U.S.A).

*Z. Li and Y. Zhang contributed equally to this work.

✉ Corresponding author: Prof. Dr. Gang Han, E-mail: Gang.Han@umassmed.edu.

Abstract

Calcium Fluoride (CaF_2) based luminescent nanoparticles exhibit unique, outstanding luminescent properties, and represent promising candidates as nanoplatforms for theranostic applications. There is an urgent need to facilitate their further development and applications in diagnostics and therapeutics as a novel class of nanotools. Here, in this critical review, we outlined the recent significant progresses made in CaF_2-related nanoparticles: Firstly, their physical chemical properties, synthesis chemistry, and nanostructure fabrication are summarized. Secondly, their applications in deep tissue bio-detection, drug delivery, imaging, cell labeling, and therapy are reviewed. The exploration of CaF_2-based luminescent nanoparticles as multifunctional nanoscale carriers for imaging-guided therapy is also presented. Finally, we discuss the challenges and opportunities in the development of such CaF_2-based platform for future development in regard to its theranostic applications.

Key words: Calcium Fluoride, luminescent nanoparticles

1. Introduction

Optical nanoparticles (NPs) are of vital importance in cutting-edge biomedical applications [1-4]. The United Nations has acknowledged the role of light in everyday life and the future by proclaiming 2015 the International Year of Light and Light-based Technologies (http://www.light2015.org/home.html). Scientists have put tremendous effort into developing NPs with diverse optical properties for theranostic applications, because of their unique properties and promising advantages in analysis, drug delivery, imaging, and therapy.[5-8] The development of NP-based imaging and therapy has originated a new term; theranostic nanomedicine.[9-12] Rare-earth- (RE) doped NPs are particular stars in this category because of the enriched spectral properties of lanthanide ions.[13-18] Numerous RE-doped NPs, especially $NaYF_4$-related NPs, were synthesized and applied in a wide range of biomedical applications in recent years because of

their down/up-conversion luminescence properties.[19-24] CaF_2 NPs represent another important outstanding luminescent matrix that has made significant progress toward theranostic applications, however, they have not yet received enough attention. CaF_2 is abundant in nature and has been known to mankind for hundreds of years; it possesses unique optical properties and was widely utilized as an outstanding luminescent matrix. In recent years, doped CaF_2 NPs were applied in theranostics such as diagnostic analysis [25], optical imaging [26,27], cell labeling [28], drug delivery [29], and tumor therapy [30,31], as shown in **Figure 1**, however, such important category of nanoparticles was surprisingly underappreciated and the related work was seldom reviewed. Indeed, there is an urgent need to outline the current results to facilitate further developments of CaF_2 NPs in theranostics.
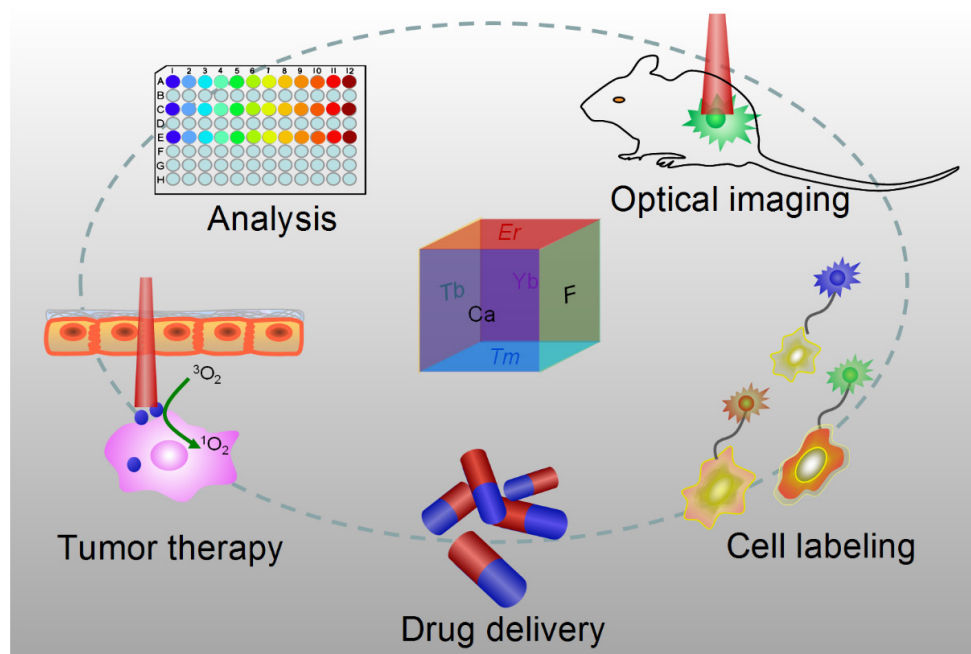
Figure 1. Applications of CaF₂-based nanoparticles. In this mini-review, we will introduce the advantages of CaF₂ as a luminescent matrix, its synthesis methods, newly developed nanostructures, and theranostic applications. The synthetic chemistry and theranostic applications of CaF₂-based up-conversion NPs (UCNPs) are especially emphasized, and include some discussion on photoluminescence of down-converting CaF₂:Ce,Tb NPs.

2. Advantages of calcium fluoride as an optical matrix

Natural fluorite, the mineral form of calcium fluoride, contains natural dopants, which generate a colorful appearance and fluorescence under UV excitation (and sometimes, phosphorescence). From this appearance arises the name, fluorite, which means *fluorescent stone*. Clear, transparent natural fluorite can be used to produce high-quality lenses in microscopes and telescopes, because of its low chromatic aberration. Fluorite optics are also used in the far-UV range (e.g., UV-C), where conventional glasses are too absorbent. Generally, CaF₂ has six main advantages in comparison with other phosphor matrices. (i) The crystal structure of CaF₂ is well-studied. CaF₂ exists naturally as a mineral named fluorite that was known to mankind for hundreds of years. The CaF₂ crystal possesses a well-known cubic structure with a face-centered lattice [space group: $Fm3m$ (225)] and a lattice parameter of a = 5.4355 Å (JCPDS 772096), in which Ca²⁺ ions lie at the nodes, while F⁻ ions lie at the centers of the octants (**Figure 2 a**). (ii) CaF₂ is optically transparent in a wide spectral range from UV, through the visible, to NIR. The edge of the fundamental absorption band of CaF₂ lies in the vacuum UV at *ca.* 12 eV, which makes CaF₂ a transparent matrix in the UV-visible–NIR region and makes CaF₂ a unique luminescent matrix in the study of optical properties of luminescent ions [13,32-38].

Figure 2 b shows a typical transparent glasslike CaF₂:Yb ceramic reported by Mortier's group.[32] (iii) CaF₂ can easily be doped with lanthanide ions. The radius of Ca²⁺ is quite close to those of lanthanide ions (**Table 1**), which makes CaF₂ a unique candidate for a luminescent matrix for lanthanide dopants that offers enriched luminescence properties for cancer diagnosis and therapy.[39] CaF₂ was used as an attractive host for phosphors with interesting up/down-conversion luminescent properties.[40-42] (iv) CaF₂ is chemically stable and has quite a low solubility product constant, K_{sp} = 3.9 × 10⁻¹¹, which particularly favor for nanocrystal growth; it is highly stable in physiological conditions, even in some harsh acidic conditions. These properties explain why F⁻ is added to commercial toothpastes to prevent dental caries; it is believed that a thin anti-acid CaF₂ coating on the enamel of teeth prevents surface corrosion. (v) CaF₂ is biocompatible. CaF₂ contains no toxic heavy metals and is essential mineral components on the surface of tooth and bones. Thus, good biocompatibility can be expected. Jaque and Speghini's group found no noticeable toxic effect of citrate-capped CaF₂:Yb,Tm and citrate-capped CaF₂:Yb,Er NPs to HeLa cells and mesenchymal stem cells over 18 h incubation.[26] Nair and Menon's group demonstrated that both CaF₂:Eu and citrate-capped CaF₂:Eu NPs (1 mM) had no obvious cytotoxicity to KB, L929, NIH 3t3, or A431 cell lines in a series of cell viability tests.[43] (vi) CaF₂ is easy to access. Unlike other phosphor matrixes that

often contain rare earth metals, such as LaF_3, YF_3, $NaYF_4$, $NaGdF_4$, and $NaLuF_4$, calcium containing compounds are easily accessible as it is abundant on earth. Its application could relieve the increasing dependence on precious rare-earth resources in the production of high-quality luminescent NPs.
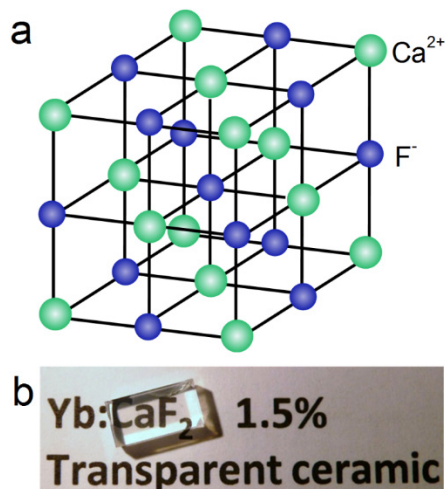

Figure 2. (a) Crystalline structure of cubic CaF_2; (b) optical image of a transparent CaF_2:Yb ceramic. Reproduced with permission from ref. [32]. Copyright (2016) Wiley-VCH.

Table 1. Radii of some alkaline-earth and rare-earth ions.

Ion	Radius/Å	Ion	Radius/Å
Mg^{2+}	0.66	Ho^{3+}	0.89
Ca^{2+}	0.99	Er^{3+}	0.88
Sr^{2+}	1.12	Tm^{3+}	0.87
Ba^{2+}	1.34	Yb^{3+}	0.86

3. Synthesis of CaF₂-based luminescent NPs

3.1 Doped CaF₂ NPs

Much is known about the structures and properties of fluorite and its derivative compounds. Fluorite has been known for hundreds of years. Early researches were mainly on its applications in radiometers used to detect human exposure doses of high-energy radiation, such as X-rays, γ-rays, α-particles, or β-particles [33,35,38,44,45]. The studies on fluorite's nano-counterparts only started in modern times. In 2003, Li's group reported the synthesis of single crystal CaF_2 nanocubes through a simple precipitation and hydrothermal procedure with no surfactants [42]. NaF and $Ca(NO_3)_2$ aqueous solution were used as the sources of F⁻ and Ca^{2+},

respectively. Amorphous CaF_2 precipitate was formed by mixing the precursor solutions. CaF_2 nanocubes were obtained after 10–20 h of hydrothermal treatment at 120 °C. The X-ray diffraction pattern of the nanocubes indicates a pure face-centered-cubic phase CaF_2 (space group: Fm3m (225)) with lattice constant a = 5.44 Å, consistent with standard JCPDS card no. 772096, as shown in **Figure 3 a**. The TEM also shows a nanocube morphology with a mean edge length of 350 ± 30 nm (inset of **Figure 3 a**). Although Li's group reported the synthesis of Eu- or Tb-doped CaF_2 nanocubes following a post-annealing procedure, the colloidal luminescent lanthanide-doped nanocubes were not yet developed then. In 2009, the same group developed sub-10 nm monodispersed CaF_2:Yb,Er UCNPs according to their liquid–solid–solution (LSS) strategy (**Figure 3 b**).[46] The as-synthesized UCNPs are able to be transparently dispersed in cyclohexane and present green UC luminescence under 980-nm laser excitation, as shown in **Figure 3 c**. The UC spectrum shows peaks mainly at 524, 541, and 654 nm that correspond to the $^2H_{11/2}$ to $^4I_{15/2}$, $^4S_{3/2}$ to $^4I_{15/2}$, and $^4F_{9/2}$ to $^4I_{15/2}$ transitions of Er^{3+}, respectively. More importantly, the UC intensity of CaF_2:Yb,Er nanocubes seems much stronger than that of sub-10-nm cubic α-$NaYF_4$:Yb,Er.

Other routes to small fluorite nanoparticles have been documented. In 2013, Chen's group developed a high-temperature organic-phase colloidal synthesis method to generate sub-10-nm lanthanide-doped CaF_2 photoluminescence/UC nanocubes.[25] 1-octadecene was used as solvent and oleic acid as a surfactant. $Ca(CH_3COO)_2 \cdot H_2O$ and lanthanide acetates were dissolved in oleic acid/1-octadecene solution as the metal precursor solution. NH_4F and NaOH methanol solution were used as the F⁻ precursor and added in metal precursor to give doped nanoprecipitation. High-quality doped CaF_2 nanocubes were obtained at 280 °C. The size of the as-synthesized NPs is only *ca.* 3.8 nm with a narrow size distribution that results in a transparent colloidal solution (**Figure 3 d**). The luminescence was downshifted by doping the NPs with Ce and Tb, while UC was realized by doping with Yb/Er (yellow) or Yb/Tm (blue) (**Figure 3 e–g**). An inert undoped CaF_2 outer shell was grown on the luminescent doped CaF_2 core to improve the UC intensity; this formed core@shell structures like (CaF_2:Yb,Er)@CaF_2 and (CaF_2:Yb,Tm)@CaF_2. As the size of the core is quite small (**Figure 3 h**), the final core@shell NPs were still sub-10 nm (**Figure 3 i**), which is difficult to obtain for β-$NaYF_4$-based core@shell structures even today. The core@shell structure was confirmed by the high-angle annular dark-field scanning transmission electron

microscopy (TEM) image. The white color was caused by the heavy element Yb, while the gray shell arises from the Ca. The phase transition of the CaF_2 nanocubes from cyclohexane to water was realized by a simple $NOBF_4$ treatment for onward applications. Another progress was reported by Tsang's group,[47] who synthesized CaF_2 UCNPs by using an oleic acid assisted hydrothermal method at 190 °C. This hydrothermal method possesses advantages in that neither N_2 atmosphere nor high-temperature manipulation is needed. The precursor is sealed in the autoclave at room temperature and then put into an oven. However, the hydrothermal reaction is tedious, and it is difficult to obtain a defined core@shell structure with good colloidal dispersibility.

Some other efforts were also made to improve the luminescent properties of CaF_2 NPs by co-doping with nonluminescent alkali ions. Chen *et al.* found that the luminescence of CaF_2:Ce,Tb can be significantly enhanced by Na^+.[25] Zhao *et al.* systematically studied the influence of alkali ion co-doping on the UC emission of CaF_2:Yb,Er.[48] They found that the UC emission can be significantly enhanced by alkali ion co-doping following a sequence of $Cs^+ > Rb^+ > K^+ > Na^+ > Li^+ >$ non-doping. They assigned the alkali ion sensitization effect to the possible change of environmental structure induced by alkali ion co-doping in the CaF_2 host. Mudring and colleagues reported enhanced luminescence in Li/Na/K co-doped alkaline earth nanofluorides.[49] Generally, monovalent Li/Na/K cations (A^+,) are incorporated (doped) into the divalent CaF_2 (Ca^{2+}) matrix structure so as to compromise/trade-off the additional positive charge of trivalent lanthanide ions (Ln^{3+}). This charge-compensation mechanism was proposed in order to explain the influence of alkali ion doping.

3.2 (Doped-CaF₂)@NaREF₄

The synthesis of CaF_2 has advantages in terms of size control, especially within the sub-10-nm regime. However, its luminescence efficiency is generally very weak due to the small size of the particles. A homogeneous core@shell structure, with the same matrix in both the active core and inert shell, is popularly applied to enhance the luminescence properties of nanoparticles. Interestingly, Zhou and Tsang's group [43] found that the blue/UV UC luminescence of CaF_2:Yb,Tm can be significantly enhanced by epitaxial growth of an inert α-$NaYF_4$ shell layer and further enhanced by an active α-$NaYF_4$:Yb shell layer. The size of the core@shell NPs only reached 9.1 nm; here we see a clear benefit of the ultrasmall CaF_2 core. The inert $NaYF_4$ shell layer can efficiently isolate the Tm emitters in the CaF_2 core from being quenched by the surface quenchers and consequently enhance their UV/blue emissions. A $NaYF_4$:Yb active shell can not only block the surface quenching of the luminescent Tm emitters, but also absorb and transfer more excitation energy to the Tm emitters in the CaF_2 core. Thus, further enhancement of the UC emission can be achieved in the core@(active shell) UCNPs. A similar phenomenon was also found in (CaF_2:Yb,Tm,Ho)@($NaYF_4$:Yb) with white UC luminescence by the same group.[47]
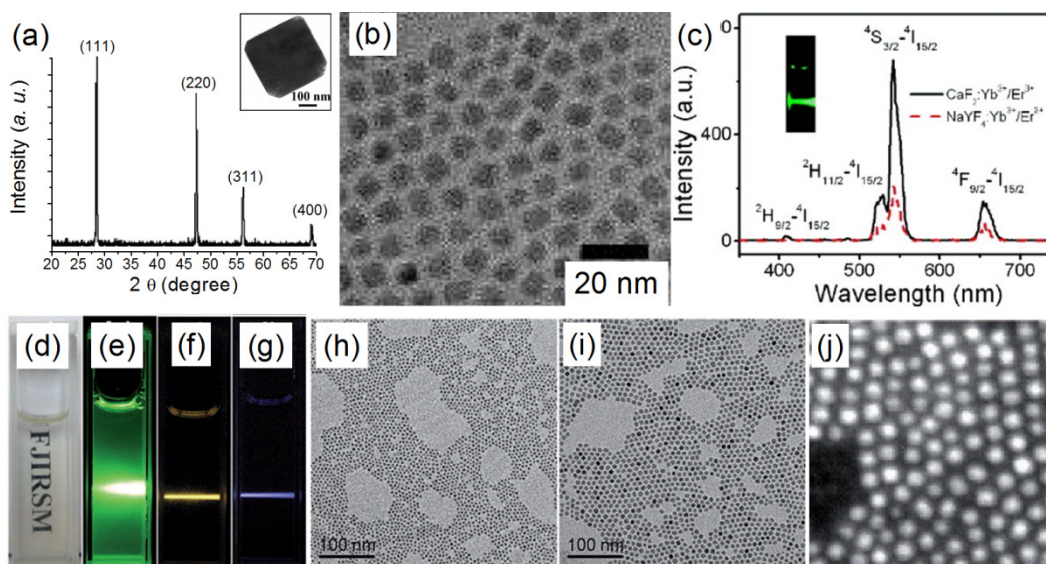

Figure 3. (a) XRD of CaF_2 nanocubes, the inset is a TEM picture of a single nanocube[42]; (b) TEM of CaF_2:Yb,Er nanocubes and (c) the corresponding upconversion spectra of doped CaF_2 vs. cubic $NaYF_4$:Yb,Er[46]; (d) the optical image of doped CaF_2 nanocubes dispersed in cyclohexane and (e) downshifting luminescence spectrum of CaF_2:Ce,Tb nanocubes in cyclohexane excited at 280 nm; (f) upconversion spectra of (CaF_2:Yb,Er)@CaF_2 and (g) (CaF_2:Yb,Tm)@CaF_2 nanocubes; (h) typical TEM images of CaF_2:Yb,Er nanocubes, (i) (CaF_2:Yb,Er)@CaF_2 and (j) a high-angle annular dark-field scanning TEM image of CaF_2:Yb,Er@CaF_2 nanocubes synthesized by a hydrothermal method; (d–j) were adopted from ref. [25]. Reproduced by permission of The Royal Society of Chemistry (2003), copyrights (2009) American Chemical Society and (2013) John Wiley and Sons.
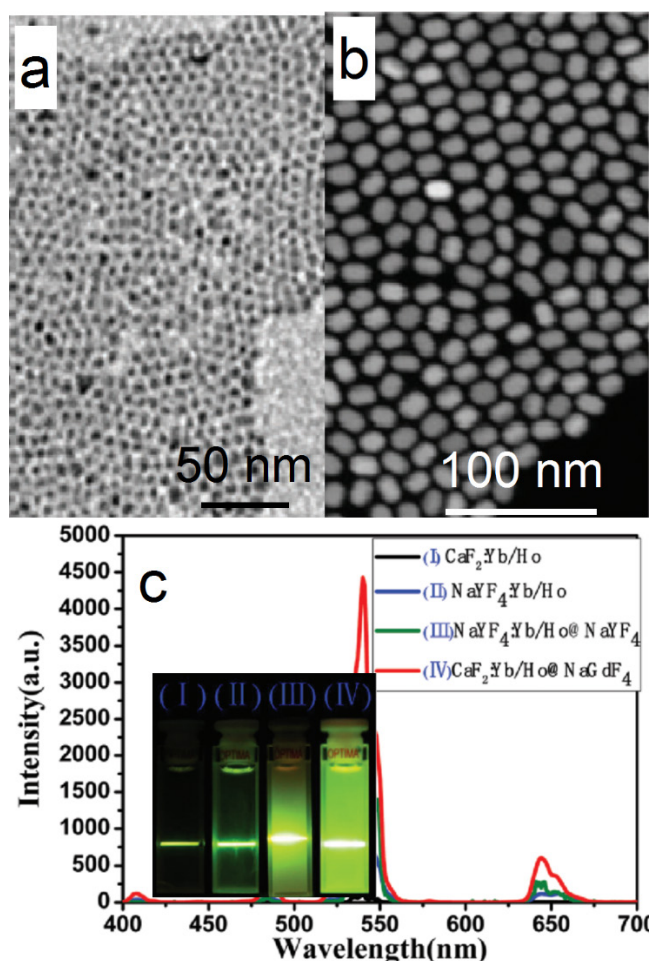
Figure 4. TEM images of (a) CaF$_2$:Yb,Ho (core) and (b) (CaF$_2$:Yb,Ho)@NaGdF$_4$ (core@shell); (c) the up-conversion spectra of doped CaF$_2$ core and core@shell NPs reported by Yang and Chen's group in 2015[51]. Reproduced by permission of The Royal Society of Chemistry(2015).

is an inert shell layer, such an impressive enhancement undoubtedly arises from suppression of surface-quenching effects on the surface of the luminescent core. The ultrasmall 4 nm CaF$_2$:Yb,Ho will expose most of the sensitizer (Yb) and activator (Ho) to the surface-quenching effects due to their extremely high "surface-to-volume" area. A thick inert shell layer not only eliminates the quenching sites of the core surface but also blocks the outer environmental quenching factors. Furthermore, the ultrasmall CaF$_2$ core can facilitate size control of the final core@shell UCNPs.

3.3 (Doped-NaREF$_4$)@CaF$_2$

CaF$_2$ can not only act as an efficient luminescent matrix, but also an efficient shell layer in the fabrication of efficient luminescent core@shell nanoparticles. Yan's group reported a facile way to achieve ultrasmall (α-NaYF$_4$:Yb,Er)@CaF$_2$ UCNPs with the pristine α-NaYF$_4$:Yb,Er NPs.[52] The CaF$_2$ shell can protect the rare-earth ions from leaking in a simulated physiological environment. The size of α-NaYF$_4$:Yb,Er can be easily controlled to within 10 nm (7 nm, **Figure 5 a**). Both α-NaYF$_4$:Yb,Er and CaF$_2$ are cubic phase and have similar crystal parameters, so CaF$_2$ can be efficiently coated onto α-NaYF$_4$:Yb,Er by means of epitaxial growth. The obtained (α-NaYF$_4$:Yb,Er)@CaF$_2$ UCNPs are *ca.* 10 nm (**Figure 5 b**). The high-angle annular dark-field scanning TEM picture shows a clear core@shell nanostructure in **Figure 5 c**. The UC emission of α-NaYF$_4$:Yb,Er can be significantly enhanced by increasing the shell thickness of CaF$_2$ (**Figure 5 d**). (α-NaYF$_4$:Yb,Er)@CaF$_2$ possesses much stronger UC emission than that of β-NaYF$_4$:Yb,Er. (α-NaYF$_4$:Yb,Er)@CaF$_2$ possesses weaker green emission but stronger red emission than classic (β-NaYF$_4$:Yb,Er)@β-NaYF$_4$ (**Figure 5 e**). The size of the classic (β-NaYF$_4$:Yb,Er)@β-NaYF$_4$ is much greater than that of (α-NaYF$_4$:Yb,Er)@CaF$_2$. The advantages of CaF$_2$ as shell are also found in (α-NaYF$_4$:Yb,Tm)@CaF$_2$ and (α-NaYF$_4$:Yb,Ho)@CaF$_2$, as shown in **Figure 5 f** and **g**.

For UV UC luminescence, (β-NaYF$_4$@Yb,Tm)@β-NaYF$_4$ was once a classic composition, in which the concentration of Yb was controlled within 20–30%.[53-63] It is not easy to control the size and morphology of high Yb doping (> 60%) β-phase NPs using common recipe.[64] Such size distortion is possibly due to delayed nucleation kinetics, according to the *La Mer* model, i.e. slow nucleation with small amount of nuclei followed by fast growth process. In addition, the required high laser power density and the concomitant heat side effects have obviously hindered the applications of such system. To conquer this obstacle, CaF$_2$ UCNPs have been developed as an

Similarly, Hao *et al*. reported heterogeneous (CaF$_2$:Yb,Ho)@NaGdF$_4$ UCNPs with significantly enhanced green UC luminescence.[51] At first, 4-nm CaF$_2$:Yb,Ho nanocubes were synthesized by using an oleic acid assisted hydrothermal method (**Figure 4 a**). Then, an inert α-NaGdF$_4$ shell was grown on the CaF$_2$:Yb,Ho core to form 17-nm (CaF$_2$:Yb,Ho)@NaGdF$_4$ UCNPs (**Figure 4 b**) by using a high-temperature organic-phase colloidal synthesis method that is widely used in the synthesis of NaYF$_4$-coated UCNPs. The UC luminescence of 4-nm CaF$_2$:Yb,Ho is weaker than that of β-NaYF$_4$:Yb,Ho (18 nm). The 28-nm (β-NaYF$_4$:Yb,Ho)@β-NaYF$_4$ classic core@shell composition has stronger UC luminescence than β-NaYF$_4$:Yb,Ho (**Figure 4 c**). Surprisingly, the 17-nm heterogeneous core@shell UCNPs, (CaF$_2$:Yb,Ho)@NaGdF$_4$, possesses the strongest UC luminescence. Moreover, its size (17 nm) is comparable with that of β-NaYF$_4$:Yb,Ho (18 nm) and much smaller than that of the classic (β-NaYF$_4$:Yb,Ho)@β-NaYF$_4$ (28 nm). Since the NaGdF$_4$

alternative with high NIR-to-UV efficiency and biocompatibility. First, CaF_2 based matrix has benefits of ideal optical transparency as a traditional used glass material, high crystallizability and negligible lattice mismatch with α-NaYF$_4$. Second, CaF_2-based UCNPs can be synthesized with small size, narrow size distribution along with excellent biocompatibility. To overcome this problem, Han's group found that (α-NaYbF$_4$:Tm)@CaF$_2$, which contains 99.5% Yb in the core, possesses significantly enhanced UC luminescence in the UV region.[65] The group successfully obtained uniform (α-NaYF$_4$:Yb,Tm)@CaF$_2$ nanocubes by using a high-temperature organic-phase titration method. The nanocubes were 27 nm across, which is comparable with the size of the classic (β-NaYF$_4$@30%Yb,0.5%Tm)@β-NaYF$_4$ composition cubes (**Figure 6 a**). A high-angle annular dark-field scanning TEM image of the nanocubes shows a clear core@shell structure with quite narrow size distribution (**Figure 6 b**). The UV emission (α-NaYF$_4$:Yb,Tm)@CaF$_2$ gradually increases along with the increasing concentration of Yb-dopant from 30 to 99.5% (**Figure 6 c, d**). Due to the negligible lattice

mismatch with α-NaYF$_4$, the Yb concentration can be significantly increased in CaF_2 coated UCNPs, and generate boosted NIR light absorption. Han et al. systemically investigated and obtained a comprehensive understanding of Yb dependent upconversion enhancement in CaF$_2$-coated α-NaYF$_4$:Yb,Tm core/shell structured UCNPs.[65] The related UV output in core/shell nanoparticles can be systematically tuned and increased monotonically with the increase of Yb^{3+} doping without energy saturation via the increase of Yb concentration up to 99.5%. In comparison with the classic UCNP composition, the UV emission of (α-NaYF$_4$:Yb,Tm)@CaF$_2$ is up to five times higher than that of (β-NaYF$_4$@30%Yb,0.5%Tm)@β-NaYF$_4$. An NIR-photocleavage application concept was demonstrated based on Han's UCNP nanocubes (**Figure 6 e**). Succinimidyl ester-derivatized caged fluorescein was linked to polyethylenimine modified nanocubes. Under 980-nm laser irradiation, the caged model drug (fluorescein) was released. This kind of NIR-triggered drug-release nanoplatform has potential applications in developing traceable, targeted, and controlled drug-delivery systems.
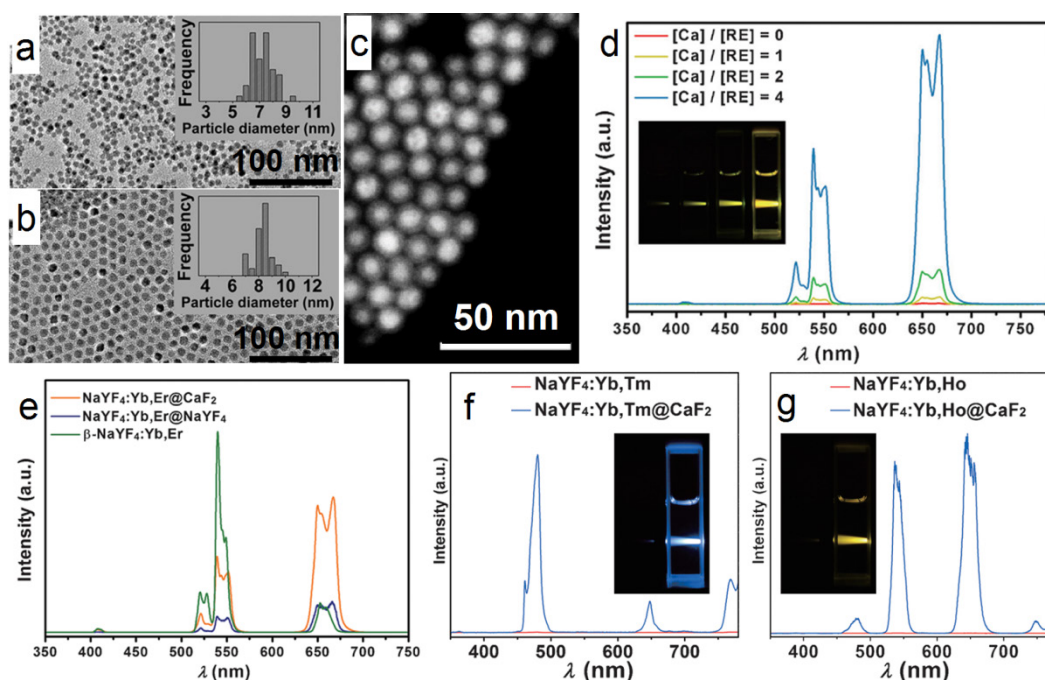

Figure 5. TEM images and size distributions of (a) the as-prepared α-NaYF$_4$:Yb,Er and (b) (α-NaYF$_4$:Yb,Er)@CaF$_2$ nanoparticles; (c) high-angle annular dark-field scanning TEM of (NaYF$_4$:Yb,Er)@CaF$_2$; (d) up-conversion spectra and digital photographs (inset) of NaYF$_4$:Yb,Er and (NaYF$_4$:Yb,Er@CaF$_2$) UCNPs with different [Ca]/[RE] molar ratios, (inset of photographs from left to right correspond to [Ca]/[RE] molar ratios of 0:1, 1:1, 2:1, and 4:1); (e) comparison between the upconversion spectra of (α-NaYF$_4$:Yb,Er)@CaF$_2$ NPs, (β-NaYF$_4$:Yb,Er)@β-NaYF$_4$ NPs, and β-NaYF$_4$:Yb,Er NPs (*ca.* 30-nm diameter); (f) UC emission spectra and digital photographs (inset) of NaYF$_4$:Yb,Tm and (NaYF$_4$:Yb,Tm)@CaF$_2$ NPs; and (g) NaYF$_4$:Yb,Ho and (NaYF$_4$:Yb,Ho)@CaF$_2$ NPs. Reproduced with permission from ref. [52]. Copyright (2012) John Wiley and Sons.

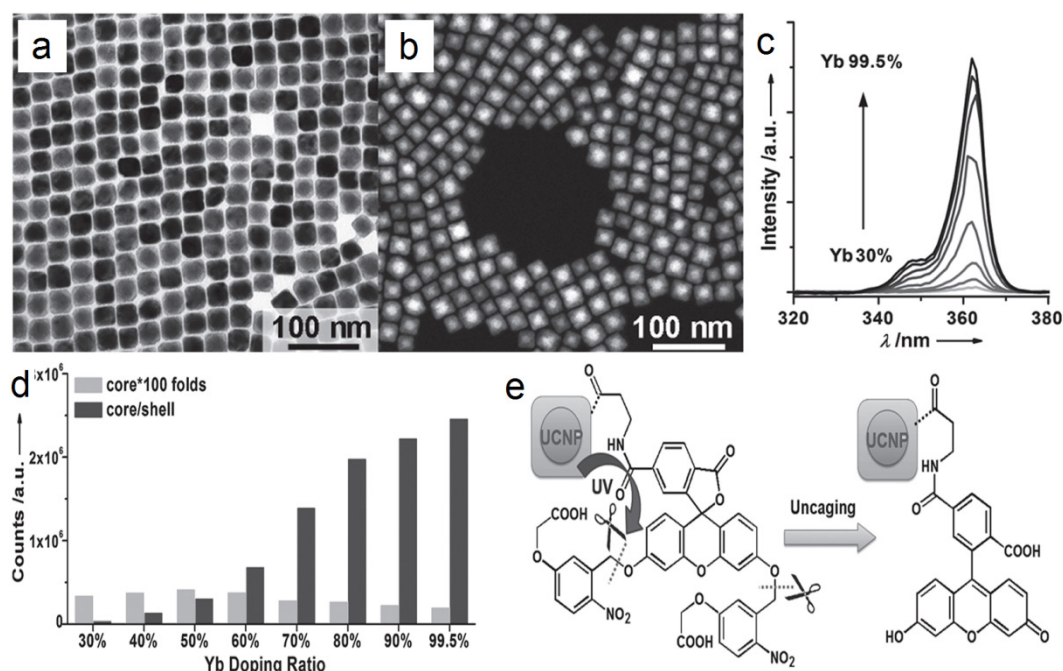**Figure 6**. (a) TEM and (b) high-angle annular dark-field scanning TEM image of (α-NaYbF₄:0.5%Tm)@CaF₂ UCNPs; (c) UC spectra of (α-NaYbF₄:0.5%Tm)@CaF₂ with different Yb levels; (d) UC emission counts of core and core/shell UCNPs series under 2.6 W cm⁻² 975-nm laser excitation; (e) Schematic illustration of NIR-triggered release of cargoes (fluorescein) on UCNPs. Reproduced with permission from ref. [65]. Copyright (2013) John Wiley and Sons.
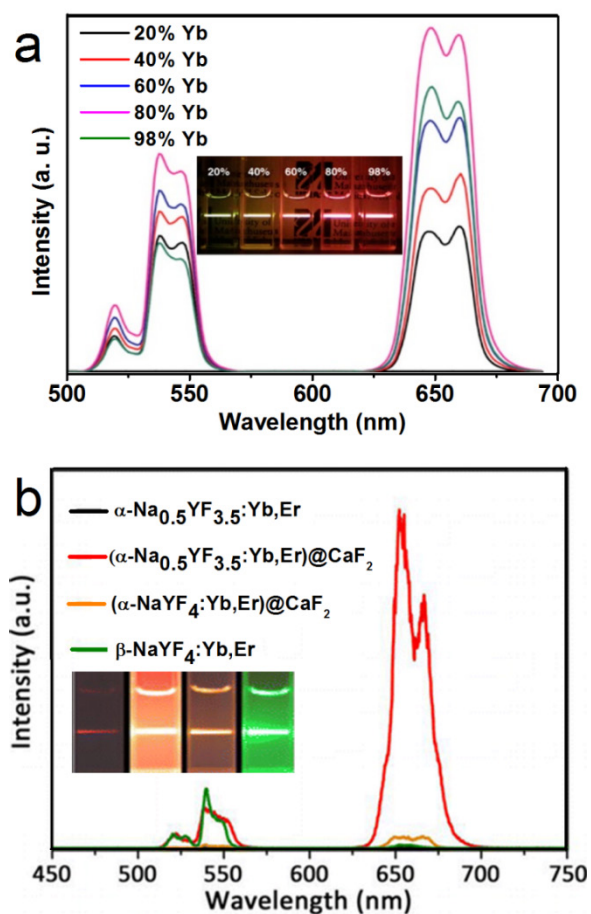

Figure 7. (a) UC spectra of (α-NaYF₄:Yb,Er)@CaF₂ with high doping concentration of Yb; (b) tailoring red/green UC ratio of CaF₂-capped UCNPs by inducing Na/F vacancies in the α-NaYF₄:Yb,Er core. Reproduced with permission from ref. [31], [66]. Copyright (2014) and (2015) American Chemical Society.

In another report of Han's group, significantly enhanced red UC can be realized in (α-NaYF₄:Yb,Er)@CaF₂ by increasing the doping concentration of Yb from 20 to 80% (**Figure 7a**).[31] The optimal composition, (α-NaYF₄:80%Yb,2%Er)@CaF₂, has a high absolute UC quantum yield of 3.2%, which is 15 times higher than the known optimal β-phase core@shell UCNPs. Further, to increase the spectrum purity, Sun and Yan's group found that a high red/green ratio can be realized in CaF₂-coated UCNPs by inducing F⁻/Na⁺ vacancies in the α-NaYF₄:Yb,Er core.[66] In an optimal composition, (α-Na₀.₅YF₃.₅:20%Yb,2%Er)@CaF₂, the red emission increased by 450 times compared with that of the α-core. Compared with larger β-NaYF₄:Yb,Er (50 nm) and stoichiometric (α-NaYF:20%Yb,2%Er)@CaF₂, (α-Na₀.₅YF₃.₅:20%Yb,2%Er)@CaF₂ possesses the strongest red and overall UC emission (**Figure 7 b**). The UC emission from 17-nm (α-Na₀.₅YF₃.₅:20%Yb,2%Er)@CaF₂ is 12 times more intense than that from 26-nm β-core@shell UCNPs.

Some other alkaline earth fluoride phosphor matrixes were also developed as luminescent NPs, such as SrF₂[67-69], BaYF₅[70-72], BaGdF₅[73-77], BaLuF₅[78], and KMgF₃[79]. There is no evidence that these derivatives possess superior luminescence over classic β-NaYF₄-based core@shell UCNPs. However, improved CT imaging can be achieved by inducing Ba, while τ₁ imaging by inducing Gd into the host materials. Thus, multimodel imaging can be achieved

by applying lanthanide-doped $BaGdF_5$ NPs. In this regard, Hao's and Lin's groups achieved UC/CT/MRI tri-model imaging based on $BaGdF_5$:Yb,Er[74] and $BaGdF_5$:Yb,Tm[75] UCNPs, respectively.

4. Theranostic applications of CaF₂-based luminescent nanoparticles

The combination of nanotechnology and molecular biology has developed into an emerging research field known as nanobiotechnology.[80] A similar term, biomedical nanotechnology, refers to the use of nanotechnology in the medical division. Luminescent NPs with small sizes are of particular interests for imaging-guided drug delivery, cancer diagnosis, and related treatments. To apply nanobased materials in biology and medicine, several conditions must be considered. Firstly, nanomaterials must be designed to interact with proteins and cells and provide limited interference with their normal biological activities. Secondly, the surfaces of the nanomaterials must be easy to post-modify by chemical means, while maintaining their physical properties after surface modification. Finally, the nanomaterials must be bio-friendly and nontoxic. CaF_2-based NPs fit most of the criteria and are emerging as dual-purpose nanomaterials for simultaneous diagnosis and therapy, which has given rise to a new term: theranostic agents, which are used for diagnosis and therapy at the same time.

4.1 Analysis

For *in vitro* analysis and bio-sensing, sub-10-nm NPs allow free access to intracellular compartments and better clearance than do nanoparticles of larger size.[81] For this reason, Chen *et al*. fabricated monodisperse sub-10 nm CaF_2:Ce,Tb NPs with highly emissive properties, as shown in **Figure 8**.[25] Upon excitation at 304 nm, the measured absolute quantum yield reached 51±1%. A homogeneous time-resolved fluorescence resonance-energy transfer (TR-FRET) assay was later explored for protein detection to analyze the concentration of biotin and urokinase plasminogen activator receptor (uPAR). Fluorescein isothiocyanate (FITC) and CaF_2:Ce,Tb NPs were selected as acceptor and donor labels, as the excitation peak of FITC at 490 nm overlaps with the emission of Tb^{3+} at 491 nm. TR-FRET was built in the avidin–biotin and uPAR–ATF pairs. The calibration curve plotted for analyst concentration shows that the TR-FRET signal of FITC/Tb^{3+} increases gradually and accordingly with the commencement of analyst concentration. Typically, the uPAR detection limit can go as low as 328 pM, which is comparable to the uPAR level in the serum of cancer patients and thus allows this method to be particular useful in sensitive cancer diagnosis.
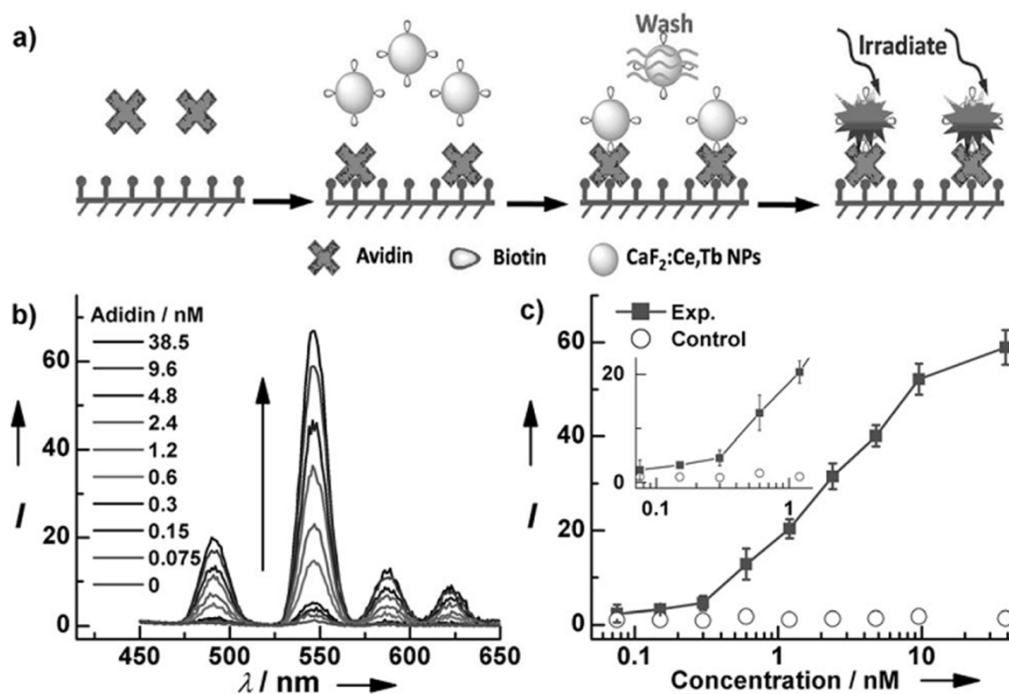

Figure 8. (a) Schematic representation of heterogeneous time-resolved photoluminescence detection of avidin; (b) time resolved photoluminescence spectra of the bioassays with biotinylated CaF_2:Ce,Tb NPs as probes as a function of avidin concentration; (c) calibrated curve for TRPL detection. Reproduced with permission from ref. [25]. Copyright (2013) John Wiley and Sons.
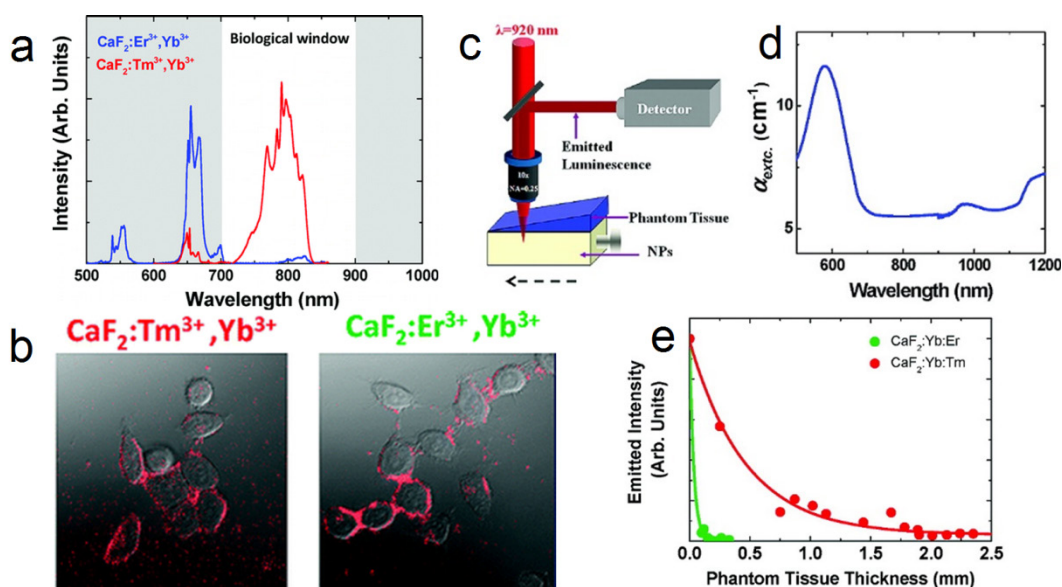
Figure 9. (a) UC spectra of CaF$_2$:Yb,Er and CaF$_2$:Yb,Tm NPs; (b) two-photon cell imaging; (c) scheme of the deep-tissue-penetration experimental setup of two-photon-excited CaF$_2$ NPs; (d) extinction spectrum of the phantom tissue; (e) measured intensity at emission wavelength of 655 (green dots) and 790 nm (red dots). Reproduced with permission from ref. [26]. Copyright (2011) American Chemical Society.

4.2 Upconversion imaging

Upconversion NPs can lead to optical conversion efficiencies that are superior to the widely used two-photon-excited fluorophores under low power density excitation source [82]. The typical UC emission of Tm^{3+} (800 nm) is in the NIR optical imaging window (**Figure 9 a**). Jaque and Speghini's group synthesized CaF$_2$:Tm,Yb NPs with 920 to 800 nm UC.[26] The successful cell marking with CaF$_2$ UCNPs was verified by using a fast multiphoton microscope; upon excitation at 920 nm, with HeLa cancer cells and CaF$_2$:Yb,Tm/Er (**Figure 9 b**). Later on, two-photon-excited fluorescence intensity was plotted as a function of the tissue thickness in a simulated phantom setup (**Figure 9 c–e**). The results also indicate that CaF$_2$:Yb,Tm (NIR emission) has superior deep-tissue-imaging ability than CaF$_2$:Yb,Er (green emission). Although the total emission intensity drastically decreases with increasing phantom tissue thickness, significant fluorescence signals from CaF$_2$:Yb,Tm could still be observed up to a tissue thickness close to 2 mm. This tissue-penetration depth is comparable to the best one achieved so far using two-photon-excited NIR CdTe quantum dots (QDs). This result clearly established that CaF$_2$:Tm,Yb UCNPs are ideal materials for the purpose of deep-tissue bio-imaging. This experiment was based on nude CaF$_2$ NPs and much-improved deep-tissue-imaging quality can be expected when using core@shell UCNPs, which possess hundreds of times enhanced UC efficiency.

Han's group also reported (α-NaYbF$_4$:Tm)@CaF$_2$ UCNPs with enhanced 975 to 800 nm UC efficiency (**Figure 10 a–c**).[27] The CaF$_2$ shell efficiently suppresses surface quenching, to yield a quantum yield as high as 0.6±0.1% under excitation with a low power density of around 0.3 W/cm^2. These UCNPs possess a small size of 27 nm.Yet, the UC emission of these UCNPs at 800 nm is superior to that of 100-nm β-NaYbF$_4$:Tm. High contrast *in vitro* and *in vivo* imaging was realized by using these UCNPs, where excitation at around 975 nm and the UC peak at 800 nm are both within the NIR optical transmission window of biological tissues [83]. To explore the suitability of the (α-NaYbF$_4$:Tm)@CaF$_2$ NPs for *in vivo* deep-tissue imaging, UCNPs was injected into a Balb/c mouse intravenously. The hair on the back of the mouse was removed, and the mouse was imaged for *in vivo* UC emission at 3 h post-injection by using a CCD camera (Maestro fluorescence imaging system). An intense UC emission can be clearly imaged in the liver, with the peak at around 800 nm; this demonstrated that it is feasible to image and spectrally distinguish the characteristic emission of the NPs (**Figure 10 d**). Finally, to explore the possibility of imaging of UC photoluminescence (PL) from a deeper tissue, (α-NaYbF$_4$:Tm)@CaF$_2$ polymeric fibrous mesh was wrapped around a rat femur; the UC emission can penetrate the thick tissue of the operated hind leg, including the femoral bone and surrounding muscle with a total depth of about 16 mm (**Figure 10 e, f**). Further, the NP solution in a cuvette can be imaged through 3.2 cm slab of pork tissue, indicating promising imaging potential for deep tissue applications.
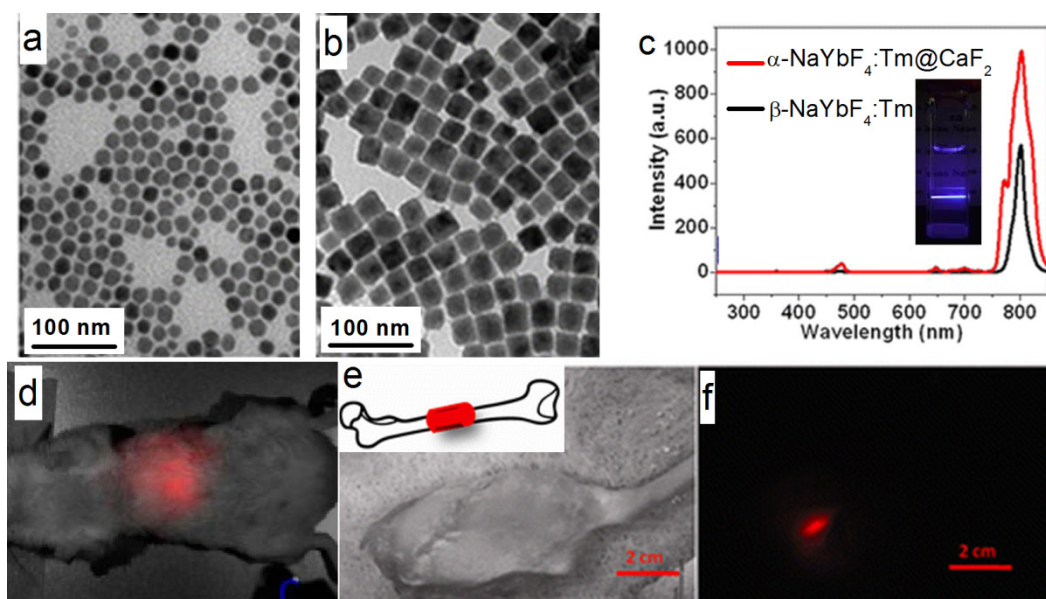
Figure 10. (a, b) TEM of α-NaYbF$_4$:Tm and (α-NaYbF$_4$:Tm)@CaF$_2$ respectively; (c) UC spectra of 27-nm (α-NaYbF$_4$:Tm)@CaF$_2$ and 100-nm β-NaYbF$_4$:Tm; the inset is the UC picture of (α-NaYbF$_4$:Tm)@CaF$_2$ in hexane; (d) *in vivo* UC imaging of (α-NaYbF$_4$:Tm)@CaF$_2$ after tail-vein injection; (e, f) deep-tissue imaging of a (α-NaYbF$_4$:Tm)@CaF$_2$ polymeric fibrous mesh wrapped around a rat femur; (e) bright field; (f) UC image. The thickness of the operated hind leg, including the femoral bone and surrounding muscle, is *ca.* 16 mm. Reproduced with permission from ref. [27]. Copyright (2012) American Chemical Society.

4.3 Cell labeling

Cell-based therapies are a major focus in regenerative medicine and tumor therapies. To facilitate the therapeutic treatment during cell therapy, the migration and differentiation of transplanted stem cells must be monitored over a long time window with high spatial resolution. In this regard, NP-based cell labeling is a useful technology [84]. *In vivo* cell tracking was realized by using magnetic NPs[85,86], fluorescent NPs[87], gold NPs[88], UCNPs[89], *etc*. Traditional optical labeling agents such as organic dyes and fluorescent NPs that emit visible light are hindered by the limited tissue penetration depth. To overcome this obstacle, Han and co-workers used (α-NaYbF$_4$:Tm)@CaF$_2$ UCNPs for rat mesenchymal stem cell (rMSCs) labeling.[28] Surface modification of UCNPs with polycationic macromolecules enables nonspecific endocytosis, and is the most commonly used strategy for shuttling NPs across cell membranes for drug delivery or cell labeling. rMSCS were labeled with UCNPs after exposing to the particles for 4 or 24 h in cell-culture media. UCNP uptake, cytoskeletal actin, and cell nuclei were visualized under a two-photon microscope with 870-nm excitation for Alexa Fluor 488 phalloidin, 980-nm excitation for UCNPs, and 690-nm excitation for 4',6-diamidino-2-phenylindole (DAPI), respectively (**Figure 11**). The UC emission was found in nearly all of the rMSCs, which demonstrates that the stem cells were successfully labeled with UCNPs. Finally, the UCNP-labeled rMSCs were allowed to differentiate along the osteogenic and adipogenic lineages upon *in vitro* induction, which suggests that the UCNP labeling did not remove or hinder these key functions of MSCs. Although the UCNP-labeled rMSCs exhibited less potent osteogenic differentiation than the unlabeled control, the potency of adipogenic differentiation was largely unaffected by UCNP labeling. Taken together, (α-NaYbF$_4$:Tm)@CaF$_2$ NPs have promising applications in cell labeling and *in vivo* tracking.
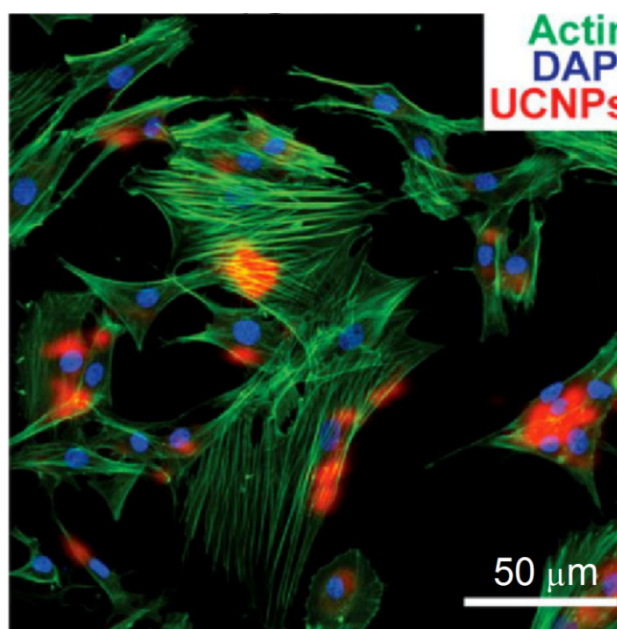

Figure 11. Co-localization of UCNP signal with rat mesenchymal stem cell actin and nuclei (labeled with DAPI) following incubation with 50 μg/mL UCNPs for 24 h. Reprinted with permission from ref. [28]. Copyright (2013) IVYSPRING.

4.4 Drug delivery

The conventional preparations of suspensions or emulsions suffer certain limitations as drug-delivery vehicles, with drawbacks such as high dose, low availability, and instability; therefore, there is a need to develop novel carriers that meet the ideal requirements of a drug-delivery system.[90-91] NPs possess many advantages as therapeutic carriers, including the potential to increase drug circulation time, enhance drug solubility, deliver preferentially to target sites, and decrease side effects.[92,93] NPs with sizes between around 10 and 200 nm can accumulate preferentially in tissues with relatively leaky vasculatures, such as tumors, through the well-known enhanced permeation and retention effect (EPR) [94]. When enriched with UC emission, the nanocarriers will possess diagnostic properties. Thus, a two-in-one theranostic nanoplatform can be prepared [8].

In this direction, Lin *et al*. demonstrated a simple, template-free, and one-step strategy for the synthesis of hollow CaF_2 spheres with controllable size by using a simple hydrothermal route [95]. The external surface of the as-synthesized CaF_2 hollow nanocomposite consists of numerous randomly aggregated and porous NPs of about 40 nm. When the lanthanide ions Ce^{3+} and Tb^{3+} were co-doped into the CaF_2 hollow spheres, the composite showed bright green photoluminescence under UV irradiation, with a quantum efficiency as high as 77%. The common painkiller and nonsteroidal anti-inflammatory drug ibuprofen (IBU), was selected as a model drug to study the storage and release properties of this carrier. A degree of IBU loading for CaF_2:Ce,Tb hollow spheres of 7.2 wt% was measured by using thermogravimetric analysis. Within 0.5 h the system showed a burst release of about 60% of IBU and the release was completed after 2 h. Generally, this monodispersed CaF_2:Ce,Tb hollow spheres can be used to encapsulate small chemical drugs and release them sufficiently, which may find potential applications in the fields of luminescence guided drug delivery and disease therapy.

Multifunctional imaging-guided drug-delivery systems were also developed based on CaF_2, while UC imaging was integrated with other imaging modalities, such as magnetic resonance (MR) and computed X-ray tomography (CT) imaging [71,74,75,96,97]. Zhao and colleagues explored the possibility of using core/shell structured alkali-ion-doped CaF_2:Yb,Er UCNPs for dual-modal UC/CT imaging.[48] Doxorubicin (DOX) was loaded and released in a controlled manner for cancer cell treatment *in vitro*. In a separate work, Lin *et al*. explored the fabrication of $Yb^{3+}/Er^{3+}/Mn^{2+}$ co-doped hollow CaF_2 nanospheres by a hydrothermal route

[29]. The nanospheres exhibit orange UC emission under NIR excitation. This platform offered huge interior space for efficacious storage and delivery of therapeutic drug. Meanwhile, the presence of Mn^{2+} and Yb^{3+} ions offered enhanced T1-weighted MR and CT imaging. Poly 2-aminoethylmethacrylate (PAMA) hydrochloride was coated onto the surface of the NPs, to facilitate the decorating of the NP with Pt(IV) prodrug via the amide linkage. The IC50 values of Pt(IV) prodrugs, cisplatin, and Pt(IV)-coated UCNPs are calculated to be 18.9, 8.2 and 2.6 µM, respectively. They show that Pt(IV)-coated CaF_2 has the strongest inhibition ability to HeLa cells. More importantly, the *in vivo* anti-tumor tests on small mice also showed that Pt(IV)-coated CaF_2 was superior to the control groups with respect to tumor suppression and reducing side effects to normal tissue. As a result, this nanocomposite combines drug delivery, UC imaging, T1-weighted MR imaging and CT imaging to provide a multifunctional platform for simultaneous tri-modal bioimaging and therapeutic applications.

4.5 Photodynamic therapy

Photodynamic therapy (PDT) is a widely recognized technique for cancer treatment in oncological, dermatological, and ophthalmic tissue, due to low cost, excellent efficiency, high drug loading, and minimal extra trauma [98,99]. A photosensitizer (PS, such as porphyrin, phthalocyanine and their derivatives) is the key component in this treatment in which reactive oxygen species (ROS) species are generated. Upon irradiation at appropriate wavelengths, PS molecules transfer excitation energy to nearby oxygen molecules, generating ROS, which consequently cause oxidative damage to nearby cancer cells. However, most PS molecules, with their huge aromatic cyclic skeleton, are hydrophobic, and this leads to aggregation in aqueous environment and hampers the loading, delivering, and generation of ROS. In addition, most PS molecules absorb strongly in the visible region and are not suitable for deep-tissue *in vivo* treatment. For these reasons, Yan *et al.* assembled the core@shell framework with (α-NaGdF$_4$:Yb,Er)@CaF$_2$NPs as the core and PS-covalently grafted mesoporous silica as the shell.[30] Moreover, the multifunctional nanomaterials utilize NIR irradiation at 980 nm to emit luminescence at about 550 and 660 nm; the former is used in fluorescence imaging and the latter is absorbed by the PS molecules to generate singlet oxygen for PDT treatment. In addition, the Gd^{3+} ions with paramagnetic properties located in the core provide a potential application as a contrast agent for MRI.

To reduce the potential toxicity of PS, Han *et al.*

conjugated an FDA-approved PDT prodrug onto the surface of UCNPs for PDT treatment. In contrast to the directly administered FDA-approved photosensitizer Photofrin, low cost 5-aminolevulinic acid (ALA) has unique advantages due to its hydrophilicity, higher selectivity in cancerous cells, and reduced concomitant photosensitivity, which leads to minimal trauma in surrounding tissue. Firstly, the red-emission from (α-NaYF$_4$:Yb,Er)@CaF$_2$ was amplified by adjusting the core Yb ratio from 20 to 98%. By doing so, the red-emission was increased 15 times with an absolute quantum yield of 3.2±0.1%, the highest reported so far (red-emission from UCNPs). [31] The prodrug ALA was conjugated to the UCNPs by means of a covalent hydrazine linkage to avoid possible preleaking of the ALA and thereby increase its bioavailability. Subsequently, with 980-nm light excitation, the optimally red-emitting UCNPs caused the PS to produce singlet oxygen and triggered tumor cell death, as seen through a deep tissue simulation (pork slab) up to 1.2 cm in thickness, both *in vitro*. Finally, *in vivo* mice models of tumors when treated with these ALA-UCNPs demonstrated significant size reduction from the controls, even under 12 mm of pork tissue (the greatest depth at which UCNP-PDT was achieved), while clinically used red light could not (**Figure 12**). These results provide new opportunities for a variety of applications using upconverting red radiation in photonics and biophotonics using bio-friendly CaF$_2$.

5. Conclusion and perspective

In sum, CaF$_2$ based luminescence NPs, possess numerous unique chemical and physical properties, i.e., superior brightness, optically transparent, apt for doping, chemically stable, biocompatible, and easy to access. To date, CaF$_2$-based NPs, especially the heterogeneous core@ shell ones, have shown their promises in numerous aspects in the field of theranostic such as analysis, deep tissue imaging, cell labeling, drug delivery, and photodynamic therapy.

Although much progress has been made, many hurdles still remain to be overcome. For example, (1) certain strategies that utilize alternative sensitizers [100], or dye antennae [101] have been developed to boost the quantum efficiency and tailor the excitation wavelengths of conventional NaYF$_4$ based UCNPs. However, these approaches have not yet been able to be implemented into CaF$_2$ based nanoparticles. (2) Effective urinary excretion and the body elimination require the nanoparticle size be smaller than 5 nm. Therefore, the novel synthesis of ultrasmall CaF$_2$ based nanoparticles that emit strong luminescence is also greatly needed (3). Their potential in vivo toxicity also needs to be further investigated. Systemic exploration of imaging performance and drug-delivery properties such as uptake, release rate, and toxicity will offer new insights for further optimizing these nanoplatforms.

Overall, although they are still under development, these CaF$_2$ based nanoparticles will provide a new set of tools that researchers can utilize from the level of a cell up to the entire animal. Ultimately, these materials may result in important new insights and therapies that are clinical relevant and currently limited by other nanomaterials.

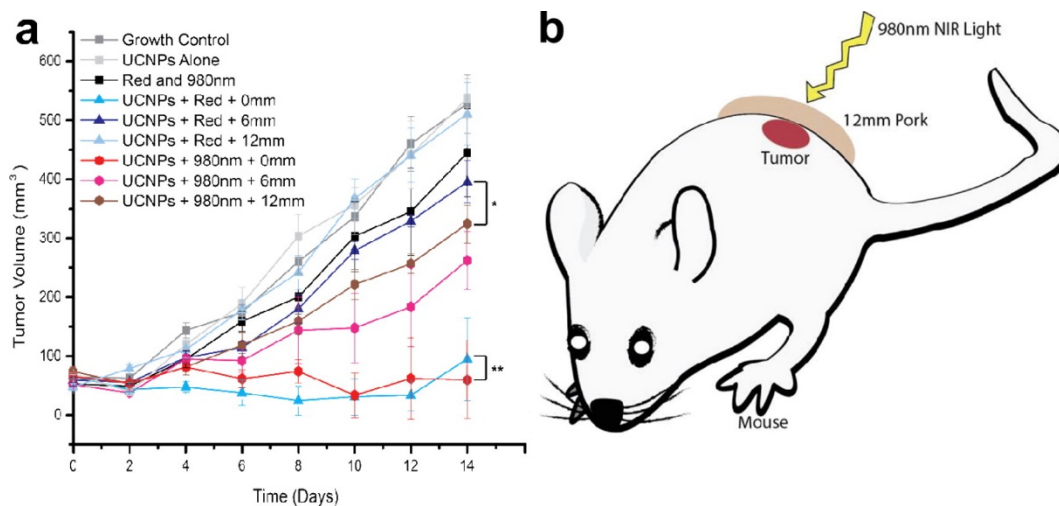
Figure 12. *In vivo* volume of tumors exposed to various controls and ALA-UCNPs with red and NIR irradiation (0.5 W/cm^2) in simulated deep tumors. Reprinted with permission from ref. [31]. Copyright (2014) American Chemical Society.

Acknowledgements

Competing Interests

The authors have declared that no competing interest exists.

References

1. Le NDB, Yazdani M, Rotello VM. Array-based sensing using nanoparticles: an alternative approach for cancer diagnostics. Nanomedicine-UK 2014, 9(10):1487-98.
2. McVey BFP, Tilley RD. Solution Synthesis, Optical Properties, and Bioimaging Applications of Silicon Nanocrystals. Accounts Chem Res 2014, 47(10):3045-51.
3. Lim SY, Shen W, Gao ZQ. Carbon quantum dots and their applications. Chem Soc Rev 2015, 44(1):362-81.
4. Idris NM, Jayakumar MKG, Bansal A, Zhang Y. Upconversion nanoparticles as versatile light nanotransducers for photoactivation applications. Chem Soc Rev 2015, 44(6):1449-78.
5. Wolfbeis OS. An overview of nanoparticles commonly used in fluorescent bioimaging. Chem Soc Rev 2015, 44(14):4743-68.
6. Wu XM, Zhu WH. Stability enhancement of fluorophores for lighting up practical application in bioimaging. Chem Soc Rev 2015, 44(13):4179-84.
7. Peng HS, Chiu DT. Soft fluorescent nanomaterials for biological and biomedical imaging. Chem Soc Rev 2015, 44(14):4699-722.
8. Xie J, Lee S, Chen XY. Nanoparticle-based theranostic agents. Adv Drug Deliver Rev 2010, 62(11):1064-79.
9. Prabhu P, Patravale V. The Upcoming Field of Theranostic Nanomedicine: An Overview. J Biomed Nanotechnol 2012, 8(6):859-82.
10. Chen XY, Gambhlr SS, Cheon J. Theranostic Nanomedicine. Accounts Chem Res 2011, 44(10):841-41.
11. Lammers T, Aime S, Hennink WE, Storm G, Kiessling F. Theranostic Nanomedicine. Accounts Chem Res 2011, 44(10):1029-38.
12. Sumer B, Gao JM. Theranostic nanomedicine for cancer. Nanomedicine-UK 2008, 3(2):137-40.
13. Liu ZD, Mei BC, Song JH, Yi GQ. Influence of Yb Concentration on the Optical Properties of CaF_2 Transparent Ceramics Codoped with Er and Yb. J Am Ceram Soc 2015, 98(12):3905-10.
14. Li ZJ, Zhang YW, La HE, Zhu R, El-Banna G, Wei YZ, et al. Upconverting NIR Photons for Bioimaging. Nanomaterials-Basel 2015, 5(4):2148-68.
15. Montalti M, Cantelli A, Battistelli G. Nanodiamonds and silicon quantum dots: ultrastable and biocompatible luminescent nanoprobes for long-term bioimaging. Chem Soc Rev 2015, 44(14):4853-921.
16. Yang DM, Ma PA, Hou ZY, Cheng ZY, Li CX, Lin J. Current advances in lanthanide ion (Ln^{3+})-based upconversion nanomaterials for drug delivery. Chem Soc Rev 2015, 44(6):1416-48.
17. Zheng W, Huang P, Tu D T, Ma E, Zhu HM, Chen XY. Lanthanide-doped upconversion nano-bioprobes: electronic structures, optical properties, and biodetection. Chem Soc Rev 2015, 44: 1379-415.
18. Zheng W, Tu D T, Huang P, Zhou SY, Chen Z, Chen XY. Time-resolved luminescent biosensing based on inorganic lanthanide-doped nanoprobes. Chem Commun 2015, 51: 4129-43.
19. Wu S, Butt HJ. Near-Infrared-Sensitive Materials Based on Upconverting Nanoparticles. Adv Mater 2016, 28(6):1208-26.
20. Zhou B, Shi BY, Jin DY, Liu XG. Controlling upconversion nanocrystals for emerging applications. Nat Nanotechnol 2015, 10(11):924-36.
21. Zhou J, Liu Q, Feng W, Sun Y, Li FY. Upconversion Luminescent Materials: Advances and Applications. Chem Rev 2015, 115(1):395-465.
22. Chen X, Peng DF, Ju Q, Wang F. Photon upconversion in core-shell nanoparticles. Chem Soc Rev 2015, 44(6):1318-30.
23. Tian G, Zhang X, Gu ZJ, Zhao YL. Recent Advances in Upconversion Nanoparticles-Based Multifunctional Nanocomposites for Combined Cancer Therapy. Adv Mater 2015, 27(47):7692-712.
24. Park YI, Lee KT, Suh YD, Hyeon T. Upconverting nanoparticles: a versatile platform for wide-field two-photon microscopy and multi-modal in vivo imaging. Chem Soc Rev 2015, 44(6):1302-17.
25. Zheng W, Zhou SY, Chen Z, Hu P, Liu YS, Tu DT, et al. Sub-10nm Lanthanide-Doped CaF_2 Nanoprobes for Time-Resolved Luminescent Biodetection. Angew Chem Int Edit 2013, 52(26):6671-76.
26. Dong NN, Pedroni M, Piccinelli F, Conti G, Sbarbati A, Ramirez-Hernandez JE, et al. NIR-to-NIR Two-Photon Excited CaF_2: Tm^{3+},Yb^{3+} Nanoparticles: Multifunctional Nanoprobes for Highly Penetrating Fluorescence Bio-Imaging. Acs Nano 2011, 5(11):8665-71.
27. Chen GY, Shen J, Ohulchanskyy TY, Patel NJ, Kutikov A, Li ZP, et al. (alpha-$NaYbF_4$:Tm^{3+})/CaF_2 Core/Shell Nanoparticles with Efficient Near-Infrared to Near-Infrared Upconversion for High-Contrast Deep Tissue Bioimaging. Acs Nano 2012, 6(9):8280-87.
28. Zhao L, Kutikov A, Shen J, Duan CY, Song J, Han G. Stem Cell Labeling using Polyethylenimine Conjugated (alpha-$NaYbF_4$:Tm^{3+})/CaF_2 Upconversion Nanoparticles. Theranostics 2013, 3(4):249-57.
29. Deng XR, Dai YL, Liu JH, Zhou Y, Ma PA, Cheng ZY, et al. Multifunctional hollow CaF_2:Yb^{3+}/Er^{3+}/Mn^{2+}-poly(2-Aminoethyl methacrylate) microspheres for Pt(IV) pro-drug delivery and tri-modal imaging. Biomaterials 2015, 50:154-63.
30. Qiao XF, Zhou JC, Xiao JW, Wang YF, Sun LD, Yan CH. Triple-functional core-shell structured upconversion luminescent nanoparticles covalently grafted with photosensitizer for luminescent, magnetic resonance imaging and photodynamic therapy in vitro. Nanoscale 2012, 4(15):4611-23.
31. Punjabi A, Wu X, Tokatli-Apollon A, El-Rifai M, Lee H, Zhang YW, et al. Amplifying the Red-Emission of Upconverting Nanoparticles for Biocompatible Clinically Used Prodrug-Induced Photodynamic Therapy. Acs Nano 2014, 8(10):10621-30.
32. Sarthou J, Aballéa P, Patriarche G, Serier-Brault H, Suganuma A, Gredin P, et al. Wet-Route Synthesis and Characterization of Yb:CaF_2 Optical Ceramics. J Am Ceram Soc 2016, 99(6):1992-2000.
33. Ginther RJ. Sensitized Luminescence of CaF_2:(Ce + Mn)[1]. J Electrochem Soc 1954, 101(5):248-57.
34. Sukis DR. Thermoluminescent Properties of CaF_2 - Dy Tlds. IEEE T Nucl Sci 1971, 18(6):185-9.
35. Azorin J, Furetta C, Gutierrez A. Evaluation of the Kinetic-Parameters of CaF_2-Tm(TLD-300) Thermo-Luminescence Dosimeters. J Phys D Appl Phys 1989, 22(3):458-64.
36. Feldmann C, Roming M, Trampert K. Polyol-mediated synthesis of nanoscale CaF_2 and CaF_2: Ce,Tb. Small 2006, 2(11):1248-50.
37. Singh VS, Joshi CP, Moharil SV, Muthal PL, Dhopte SM. Modification of luminescence spectra of CaF_2: Eu^{2+}. Luminescence 2015, 30(7):1101-05.
38. Zahedifar M, Sadeghi E, Shanei MM, Sazgarnia A, Mehrabi M. Afterglow properties of CaF_2:Tm nanoparticles and its potential application in photodynamic therapy. J Lumin 2016, 171:254-58.
39. Teo RD, Termini J, Gray HB. Lanthanides: Applications in Cancer Diagnosis and Therapy. J Med Chem 2016, 59(13):6012-24.
40. Rao DN, Prasad J, Prasad PN. 2-Photon Excitation of Ho^{3+} in the CaF_2, SrF_2, and CdF_2 Lattices. Phys Rev B 1983, 28(1):20-23.
41. Bensalah A, Mortier M, Patriarche G, Gredin P, Vivien D. Synthesis and optical characterizations of undoped and rare-earth-doped CaF_2 nanoparticles. J Solid State Chem 2006, 179(8):2636-44.
42. Sun XM, Li YD. Size-controllable luminescent single crystal CaF_2 nanocubes. Chem Commun 2003, 34(14):1768-69.
43. Sasidharan S, Jayasree A, Fazal S, Koyakutty M, Nair SV, Menon D. Ambient temperature synthesis of citrate stabilized and biofunctionalized, fluorescent calcium fluoride nanocrystals for targeted labeling of cancer cells. Biomater Sci-Uk 2013, 1(3):294-305.
44. Pradhan AS. Effect of heating rate on the responses of CaF_2:Cu, CaF_2:Tm, CaF_2:Dy and CaF_2:Mn. Radiat Prot Dosim 2002, 100(1-4):289-92.
45. Kennedy SMM. Photoluminescence studies of gamma-irradiated CaF_2:Dy :Pb:Na single crystals. J Lumin 2008, 128(4):680-84.
46. Wang GF, Peng Q, Li YD. Upconversion Luminescence of Monodisperse CaF_2:Yb^{3+}/Er^{3+} Nanocrystals. J Am Chem Soc 2009, 131(40):14200-01.
47. Zhou B, Tao L, Tsang YH, Jin W. Core-shell nanoarchitecture: a strategy to significantly enhance white-light upconversion of lanthanide-doped nanoparticles. J Mater Chem C 2013, 1(28):4313-18.
48. Yin WY, Tian G, Ren WL, Yan L, Jin S, Gu ZJ, et al. Design of multifunctional alkali ion doped CaF2 upconversion nanoparticles for simultaneous bioimaging and therapy. Dalton T 2014, 43(10):3861-70.
49. Lorbeer C, Behrends F, Cybinska J, Eckert H, Mudring AV. Charge compensation in RE^{3+} (RE = Eu, Gd) and M^+ (M = Li, Na, K) co-doped alkaline earth nanofluorides obtained by microwave reaction with reactive ionic liquids leading to improved optical properties. J Mater Chem C 2014, 2(44):9439-50.
50. Tao LL, Zhou B, Jin W, Chai Y, Tang CY, Tsang YH. Improved multiphoton ultraviolet upconversion photoluminescence in ultrasmall core-shell nanocrystals. Opt Lett 2014, 39(21):6265-68.
51. Hao SW, Yang LM, Qiu HL, Fan RW, Yang CH, Chen GY. Heterogeneous core/shell fluoride nanocrystals with enhanced upconversion photoluminescence for in vivo bioimaging. Nanoscale 2015, 7(24):10775-80.
52. Wang YF, Sun LD, Xiao JW, Feng W, Zhou JC, Shen J, et al. Rare-Earth Nanoparticles with Enhanced Upconversion Emission and Suppressed Rare-Earth-Ion Leakage. Chem-Eur J 2012, 18(18):5558-64.
53. Yan B, Boyer JC, Branda NR, Zhao Y. Near-Infrared Light-Triggered Dissociation of Block Copolymer Micelles Using Upconverting Nanoparticles. J Am Chem Soc 2011, 133(49):19714-17.
54. Yang YM, Shao Q, Deng RR, Wang C, Teng X, Cheng K, Cheng Z, Huang L, Liu Z, Liu XG, Xing BG. In Vitro and In Vivo Uncaging and Bioluminescence Imaging by Using Photocaged Upconversion Nanoparticles. Angew Chem Int Edit 2012, 51(13):3125-29.

55. Jayakumar MKG, Idris NM, Zhang Y. Remote activation of biomolecules in deep tissues using near-infrared-to-UV upconversion nanotransducers. P Natl Acad Sci USA 2012, 109(22):8483-88.

56. Yang YM, Velmurugan B, Liu XG, Xing BG. NIR Photoresponsive Crosslinked Upconverting Nanocarriers Toward Selective Intracellular Drug Release. Small 2013, 9(17):2937-44.

57. Viger ML, Grossman M, Fomina N, Almutairi A. Low Power Upconverted Near-IR Light for Efficient Polymeric Nanoparticle Degradation and Cargo Release. Adv Mater 2013, 25(27):3733-38.

58. Liu G, Zhou LZ, Su Y, Dong CM. An NIR-responsive and sugar-targeted polypeptide composite nanomedicine for intracellular cancer therapy. Chem Commun 2014, 50(83):12538-41.

59. He SQ, Krippes K, Ritz S, Chen ZJ, Best A, Butt HJ, Mailander V, Wu S. Ultralow-intensity near-infrared light induces drug delivery by upconverting nanoparticles. Chem Commun 2015, 51(2):431-34.

60. Chen ZJ, He SQ, Butt HJ, Wu S. Photon Upconversion Lithography: Patterning of Biomaterials Using Near-Infrared Light. Adv Mater 2015, 27(13):2203-06.

61. Chen ZJ, Sun W, Butt HJ, Wu S. Upconverting-Nanoparticle-Assisted Photochemistry Induced by Low-Intensity Near-Infrared Light: How Low Can We Go? Chem-Eur J 2015, 21(25):9165-70.

62. Li W, Wang JS, Ren JS, Qu XG. Near-Infrared Upconversion Controls Photocaged Cell Adhesion. J Am Chem Soc 2014, 136(6):2248-51.

63. Yan B, Boyer JC, Habault D, Branda NR, Zhao Y. Near Infrared Light Triggered Release of Biomacromolecules from Hydrogels Loaded with Upconversion Nanoparticles. J Am Chem Soc 2012, 134(40):16558-61.

64. Kale V, Lastusaari M, Holsa J, Soukka T. Intense UV upconversion through highly sensitized NaRF4:Tm (R:Y,Yb) crystals. Rsc Adv 2015, 5(45):35858-65.

65. Shen J, Chen GY, Ohulchanskyy TY, Kesseli SJ, Buchholz S, Li ZP, et al. Tunable Near Infrared to Ultraviolet Upconversion Luminescence Enhancement in (alpha-NaYF$_4$:Yb,Tm)/CaF$_2$ Core/Shell Nanoparticles for In situ Real-time Recorded Biocompatible Photoactivation. Small 2013, 9(19):3213-17.

66. Dong H, Sun LD, Wang YF, Ke J, Si R, Xiao JW, et al. Efficient Tailoring of Upconversion Selectivity by Engineering Local Structure of Lanthanides in Na$_x$REF$_{3+x}$ Nanocrystals. J Am Chem Soc 2015, 137(20):6569-76.

67. Rodriguez-Sevilla P, Rodriguez-Rodriguez H, Pedroni M, Speghini A, Bettinelli M, Sole JG, et al. Assessing Single Upconverting Nanoparticle Luminescence by Optical Tweezers. Nano Lett 2015, 15(8):5068-74.

68. Quintanilla M, Cantarelli IX, Pedroni M, Speghini A, Vetrone F. Intense ultraviolet upconversion in water dispersible SrF$_2$: Tm^{3+}, Yb^{3+} nanoparticles: the effect of the environment on light emissions. J Mater Chem C 2015, 3(3):3108-13.

69. Villa I, Vedda A, Cantarelli IX, Pedroni M, Piccinelli F, Bettinelli M, et al. 1.3 um emitting SrF$_2$:Nd^{3+} nanoparticles for high contrast in vivo imaging in the second biological window. Nano Res 2015, 8(2):649-65.

70. Lei YQ, Pang M, Fan WQ, Feng J, Song SY, Dang S, et al. Microwave-assisted synthesis of hydrophilic BaYF$_5$:Tb/Ce, Tb green fluorescent colloid nanocrystals. Dalton T 2011, 40(1):142-45.

71. Zhang CM, Ma PA, Li CX, Li GG, Huang SS, Yang DM, et al. Controllable and white upconversion luminescence in BaYF$_5$:Ln^{3+} (Ln = Yb, Er, Tm) nanocrystals. J Mater Chem 2011, 21(3):717-23.

72. Liu HR, Lu W, Wang HB, Rao L, Yi ZG, Zeng SJ, et al. Simultaneous synthesis and amine-functionalization of single-phase BaYF$_5$:Yb/Er nanoprobe for dual-modal in vivo upconversion fluorescence and long-lasting X-ray computed tomography imaging. Nanoscale 2013, 5(13):6023-29.

73. Yang DM, Li CX, Li GG, Shang MM, Kang XJ, Lin J. Colloidal synthesis and remarkable enhancement of the upconversion luminescence of BaGdF$_5$:Yb^{3+}/Er^{3+} nanoparticles by active-shell modification. J Mater Chem 2011, 21(16):5923-27.

74. Zeng SJ, Tsang MK, Chan CF, Wong KL, Hao JH. PEG modified BaGdF5:Yb/Er nanoprobes for multi-modal upconversion fluorescent, in vivo X-ray computed tomography and biomagnetic imaging. Biomaterials 2012, 33(36):9232-38.

75. Yang DM, Dai YL, Liu JH, Zhou Y, Chen YY, Li CX, et al. Ultra-small BaGdF5-based upconversion nanoparticles as drug carriers and multimodal imaging probes. Biomaterials 2014, 35(6):2011-23.

76. Tsang MK, Ye WW, Wang GJ, Li JM, Yang M, Hao JH. Ultrasensitive Detection of Ebola Virus Oligonucleotide Based on Upconversion Nanoprobe/Nanoporous Membrane System. Acs Nano 2016, 10(1):598-605.

77. Zhang H, Wu HX, Wang J, Yang Y, Wu DM, Zhang YJ, et al. Graphene oxide-BaGdF$_5$ nanocomposites for multi-modal imaging and photothermal therapy. Biomaterials 2015, 42:66-77.

78. Zhang YL, Liu XH, Lang YB, Yuan Z, Zhao D, Qin GS, et al. Synthesis of ultra-small BaLuF$_5$:Yb^{3+}, Er^{3+}@BaLuF$_5$:Yb^{3+} active-core-activeshell nanoparticles with enhanced up-conversion and down-conversion luminescence by a layer-by-layer strategy. J Mater Chem C 2015, 3(9):2045-53.

79. Wu M, Song EH, Chen ZT, Ding S, Ye S, Zhou JJ, et al. Single-band red upconversion luminescence of Yb^{3+}-Er^{3+} via nonequivalent substitution in perovskite KMgF$_3$ nanocrystals. J Mater Chem C 2016, 4(8):1675-84.

80. Tan A, Rajadas J, Seifalian AM. Exosomes as nano-theranostic delivery platforms for gene therapy. Adv Drug Deliver Rev 2013, 65(3):357-67.

81. Longmire M, Choyke PL, Kobayashi H. Clearance properties of nano-sized particles and molecules as imaging agents: considerations and caveats. Nanomedicine-UK 2008, 3(5):703-17.

82. Wu X, Chen G, Shen J, li z, Zhang Y, Han G. Upconversion Nanoparticles: A Versatile Solution to Multiscale Biological Imaging. Bioconjugate Chem 2014, 26(2):166-75.

83. Nyk M, Kumar R, Ohulchanskyy TY, Bergey EJ, Prasad PN. High Contrast in Vitro and in Vivo Photoluminescence Bioimaging Using Near Infrared to Near Infrared Up-Conversion in Tm^{3+} and Yb^{3+} Doped Fluoride Nanophosphors. Nano Lett 2008, 8(11):3834-38.

84. Thu MS, Bryant LH, Coppola T, Jordan EK, Budde MD, Lewis BK, et al. Self-assembling nanocomplexes by combining ferumoxytol, heparin and protamine for cell tracking by magnetic resonance imaging. Nat Med 2012, 18(3):463-U165.

85. Bull E, Madani SY, Sheth R, Seifalian A, Green M, Seifalian AM. Stem cell tracking using iron oxide nanoparticles. Int J Nanomed 2014, 9:1641-53.

86. Edmundson M, Thanh NTK, Song B. Nanoparticles Based Stem Cell Tracking in Regenerative Medicine. Theranostics 2013, 3(8):573-82.

87. Ji XY, Peng F, Zhong YL, Su YY, Jiang XX, Song CX, et al. Highly Fluorescent, Photostable, and Ultrasmall Silicon Drug Nanocarriers for Long-Term Tumor Cell Tracking and In-Vivo Cancer Therapy. Adv Mater 2015, 27(6):1029-34.

88. Meir R, Shamalov K, Betzer O, Motiei M, Horovitz-Fried M, Yehuda R, et al. Nanomedicine for Cancer Immunotherapy: Tracking Cancer-Specific T-Cells in Vivo with Gold Nanoparticles and CT Imaging. Acs Nano 2015, 9(6):6363-72.

89. Xiang J, Xu LG, Gong H, Zhu WW, Wang C, Xu J, et al. Antigen-Loaded Upconversion Nanoparticles for Dendritic Cell Stimulation, Tracking, and Vaccination in Dendritic Cell-Based Immunotherapy. Acs Nano 2015, 9(6):6401-11.

90. Bagheri A, Arandiyan H, Boyer C, Lim M. Lanthanide-Doped Upconversion Nanoparticles: Emerging Intelligent Light-Activated Drug Delivery Systems. Adv Sci 2016, 3(7):1500437.

91. Yang DM, Ma PA, Hou ZY, Cheng ZY, Li CX, Lin J. Current advances in lanthanide ion (Ln^{3+})-based upconversion nanomaterials for drug delivery. Chem Soc Rev 2015, 44(6):1416-48.

92. Rwei AY, Wang WP, Kohane DS. Photoresponsive nanoparticles for drug delivery. Nano Today 2015, 10(4):451-67.

93. Zhu X, Radovic-Moreno AF, Wu J, Langer R, Shi JJ. Nanomedicine in the management of microbial infection - Overview and perspectives. Nano Today 2014, 9(4):478-98.

94. Albanese A, Tang PS, Chan WCW. The Effect of Nanoparticle Size, Shape, and Surface Chemistry on Biological Systems. Annu Rev Biomed Eng, 2012, 14:1-16.

95. Zhang CM, Li CX, Peng C, Chai RT, Huang SS, Yang DM, et al. Facile and Controllable Synthesis of Monodisperse CaF2 and CaF$_2$:Ce^{3+}/Tb^{3+} Hollow Spheres as Efficient Luminescent Materials and Smart Drug Carriers. Chem-Eur J 2010, 16(19):5672-80.

96. Sun MZ, Xu LG, Ma W, Wu XL, Kuang H, Wang LB, et al. Hierarchical Plasmonic Nanorods and Upconversion Core-Satellite Nanoassemblies for Multimodal Imaging-Guided Combination Phototherapy. Adv Mater 2016, 28(5):898-904.

97. Lv RC, Yang PP, He F, Gai SL, Li CX, Dai YL, et al. A Yolk-like Multifunctional Platform for Multimodal Imaging and Synergistic Therapy Triggered by a Single Near-Infrared Light. Acs Nano 2015, 9(2):1630-47.

98. Lucky SS, Soo KC, Zhang Y. Nanoparticles in Photodynamic Therapy. Chem Rev 2015, 115(4):1990-2042.

99. Ben-Nun Y, Merquiol E, Brandis A, Turk B, Scherz A, Blum G. Photodynamic Quenched Cathepsin Activity Based Probes for Cancer Detection and Macrophage Targeted Therapy. Theranostics 2015, 5(8):847-62.

100. Shen J, Chen GY, Vu AM, Fan W, Bilsel OS, Chang CC, Han G. Engineering the Upconversion Nanoparticle Excitation Wavelength: Cascade Sensitization of Tri-doped Upconversion Colloidal Nanoparticles at 800 nm. Adv Opt Mater 2013, 1 (9):644-650.

101. Wu X, Lee H, Bilsel O, Zhang YW, Li ZJ, Chen T, Liu Y, Duan CY, Shen J, Punjabi A, Han G. Tailoring dye-sensitized upconversion nanoparticle excitation bands towards excitation wavelength selective imaging. Nanoscale 2015, 7 (44):18424-18428.